Plasma Potential and Langmuir Probe Measurements in the Near-field Plume of the NASA-300M Hall Thruster

Daniel A. Herman[*], Rohit Shastry[†], Wensheng Huang[‡], George C. Soulas[§], and Hani Kamhawi[**]
NASA Glenn Research Center, Cleveland, OH, 44135

In order to aid in the design of high-power Hall thrusters and provide experimental validation for existing modeling efforts, plasma potential and Langmuir probe measurements were performed in the near-field plume of the NASA-300M Hall thruster. A probe array consisting of a Faraday probe, Langmuir probe, and emissive probe was used to interrogate the plume from approximately 0.1 – 2.0 mean thruster diameters downstream of the thruster exit plane at four operating conditions: 300 V, 400 V, and 500 V at 20 kW as well as 300 V at 10 kW. Results show that the acceleration zone and high-temperature region were contained within 0.3 mean thruster diameters from the exit plane at all operating conditions. Isothermal lines were shown to strongly follow magnetic field lines in the near-field, with maximum temperatures ranging from 19 - 27 eV. The electron temperature spatial distribution created large drops in measured floating potentials in front of the magnetic pole surfaces where the plasma density was low, which suggests strong sheaths at these surfaces. The data taken have provided valuable information for future design and modeling validation, and complements ongoing internal measurement efforts on the NASA-300M.

Nomenclature

C	=	line capacitance
$D_{T,m}$	=	mean thruster diameter
I_{cap}	=	capacitive current
$\dot{m}_a$	=	anode mass flow rate
P_d	=	discharge power
T	=	thrust
T_e	=	electron temperature
η_a	=	anode efficiency

I. Introduction

HALL thrusters are an electric propulsion technology that is becoming an increasingly attractive option for NASA manned and science missions. With an increased emphasis on higher thrust levels and reduced trip times, the Office of the Chief Technologist (OCT) has taken an interest in high-power Hall thrusters in the vicinity of 20 – 50 kW. NASA's Glenn Research Center (GRC) has had a long history of developing and testing such high-power Hall thrusters.[1-3] From this work, a number of high-power thrusters were built, including the NASA-300M, 400M, 457Mv1 and 457Mv2. Due to interest and funding from OCT, these thrusters, in particular the 300M and 457Mv2, are now being revisited and a number of measurements are being taken in order to better understand high-power Hall thruster physics and characterize performance.[4-7] The purpose of these measurements is three-fold. The first is to provide data that will help characterize thruster performance and efficiency that will ultimately lead to the design of a high-performance, high-power Hall thruster with long lifetime. The second is to provide baseline data on existing thrusters prior to planned modifications utilizing a magnetically-shielded design for long life.[8] The third

[*] Aerospace Engineer, Propulsion and Propellants Branch, 21000 Brookpark Rd., MS 86-8, Senior Member.
[†] Aerospace Engineer, Propulsion and Propellants Branch, 21000 Brookpark Rd., MS 301-3, Member.
[‡] Aerospace Engineer, Propulsion and Propellants Branch, 21000 Brookpark Rd., MS 301-3, Member.
[§] Aerospace Engineer, Propulsion and Propellants Branch, 21000 Brookpark Rd., MS 16-1, Member.
[**] Aerospace Engineer, Propulsion and Propellants Branch, 21000 Brookpark Rd., MS 301-3, Associate Fellow.

is to provide experimental data to validate existing modeling efforts at GRC and the Jet Propulsion Laboratory (JPL).[9]

To reach these goals, an electrostatic probe array was used to interrogate the near-field plume of the 20-kW NASA-300M from approximately 0.1 – 2 mean thruster diameters ($D_{T,m}$) downstream of the thruster exit plane. Similar measurements have been taken before on the 6-kW H6 Hall thruster at JPL.[10] The probe array consisted of a near-field Faraday probe, a single Langmuir probe, and two emissive probes (one for redundancy). The measurements taken with the Faraday probe are the subject of a companion paper[4] and are not discussed here. Measurements at these distances were facilitated with a high-speed linear motion table typically run between 250 and 375 mm/s, helping to ensure probe survivability in the harsh near-field environment. While data were taken at seven operating conditions over a wide range of discharge voltages and powers, only four are presented in this work: 300 V at 10 and 20 kW discharge power, 400 V at 20 kW, and the nominal operating condition of 500 V at 20 kW.

The paper is organized as follows: Section II details the vacuum facility, Hall thruster, and various probes used in this study as well as the data collection methods. Section III provides spatial maps of the measured plasma potential and electron temperature in the near-field plume at the four operating conditions listed above. Section IV discusses the isothermal line distribution, how this distribution affects the regions near the magnetic pole surfaces, behavior of the plasma potential and electron temperature in the very-near-field plume ($\leq 0.2\ D_{T,m}$), as well as symmetry between the two interrogated thruster sides. Section V summarizes the conclusions from the study.

II. Experimental Apparatus

A. Vacuum Facility

Testing for this study was performed in Vacuum Facility 5 (VF-5) at NASA GRC. The facility is a 4.6-m-diameter by 18.3-m-long cylindrical chamber that is equipped with cryogenic surfaces as well as 20 0.8-m-diameter oil diffusion pumps. Facility pressure was measured with an exposed hot-cathode ionization gauge that was mounted near the test article in order to obtain an accurate measurement of the backpressure the thruster was exposed to during operation. Facility base pressures of 4.0×10^{-7} Torr were routinely achieved. Pressure next to thruster did not exceed 2.5×10^{-5} Torr (corrected for xenon) during the extent of testing.

B. Test Article and Support Hardware

The test article for this study was the 20-kW NASA-300M Hall thruster. Performance testing of this thruster was completed in 2011 within VF-5 at NASA GRC.[5] The NASA-300M is a nominally 20-kW thruster routinely operated up to 500 V of discharge voltage as well as up to 67 A of discharge current. Xenon was supplied through commercially available mass flow controllers with an accuracy of ±1% of reading. A commercial power supply capable of outputting 2000 V and 100 A was used to sustain the discharge. Separate power supplies were used to energize the magnet coils, cathode keeper and heater. The thruster's center-mounted cathode is based on the discharge cathode assembly of NASA's Evolutionary Xenon Thruster (NEXT) and has been used with the NASA-457Mv1 and NASA-400M thrusters. The cathode flow rate was fixed at 8% of the anode flow rate throughout testing. For this study, the cathode was retracted so that it lay flush with the thruster exit plane, resulting in a slightly increased coupling voltage. This was done so that the cathode position was not a limiting factor on the closest approach of probe interrogation. A symmetric magnetic field topology (one that is symmetric about the channel centerline) was used for each operating condition presented in this work, with the field strength chosen to maximize anode efficiency as measured by a thrust stand:

$$\eta_a = \frac{T^2}{2\dot{m}_a P_d}, \tag{1}$$

where η_a is the anode efficiency, T is the thrust, $\dot{m}_a$ is the anode mass flow rate, and P_d is the discharge power.

C. Near-field Plume Diagnostics

This study utilized a multi-probe array comprised of a near-field Faraday probe, a single Langmuir probe, and two emissive probes. The additional emissive probe was added to introduce redundancy due to the fragility of this probe, thus allowing testing to continue after the primary probe failed. The near-field Faraday probe is not discussed in detail here as it is the primary subject of a companion paper.[4] Figure 1 shows the multi-probe array both prior to and during operation. The emissive probe on the opposite side of the Faraday probe was treated as the primary emissive probe, while the one next to the Langmuir probe was a backup probe. Each probe was fixed within machined compression tube fittings that mounted onto a graphite block to minimize backsputtered products.

The probe tips were mounted approximately 12.5 cm in front of the graphite block to minimize the probe array footprint close to the thruster. Each probe was spaced radially apart by approximately 30 mm. The graphite block was mounted onto a triangular frame with a square tube as the primary vertical member. This design was chosen to minimize weight as well as vibrations associated with table movement while maintaining structural rigidity.

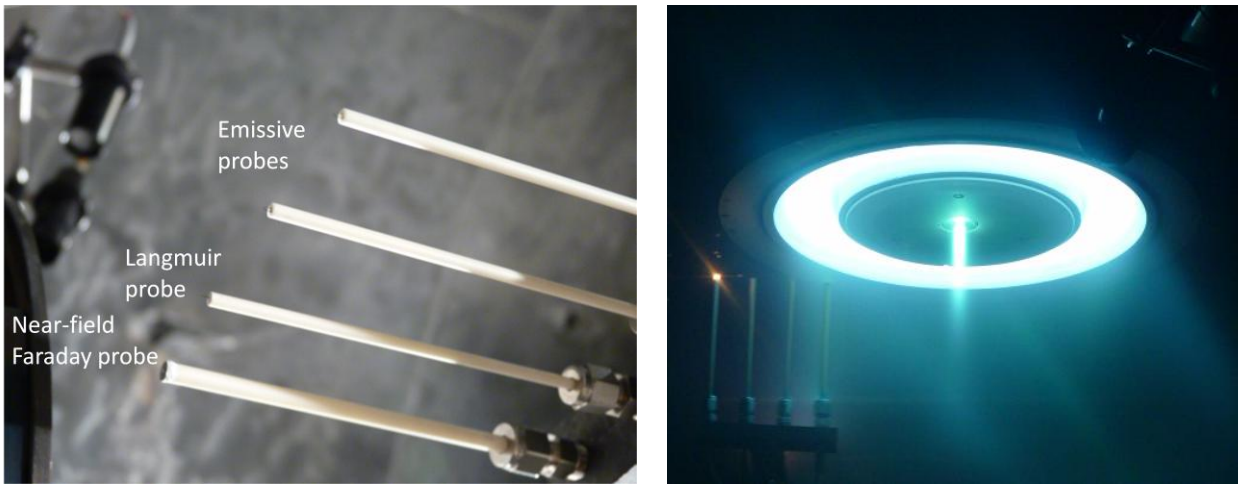

Figure 1. Photographs of the probe array used in this study. Left: Photograph showing order of four probes within array, prior to operation. Right: Array sweeping near the thruster exit plane of the 300M (array is shown to the left of thruster).

The multi-probe array was mounted onto a commercially available belt-driven 2-axis motion table system. The radial motion table was run at high speed to minimize probe residence time in the near-field plume. Typical speeds ranged from 250 – 375 mm/s. The probe array was run from end to end in the radial direction, resulting in data approximately 4 $D_{T,m}$ in either direction from thruster centerline. The axial interrogation grid was chosen to provide fine resolution near the exit plane where large gradients were expected, with gradually increasing step sizes as the probes moved further downstream (see Fig. 2).

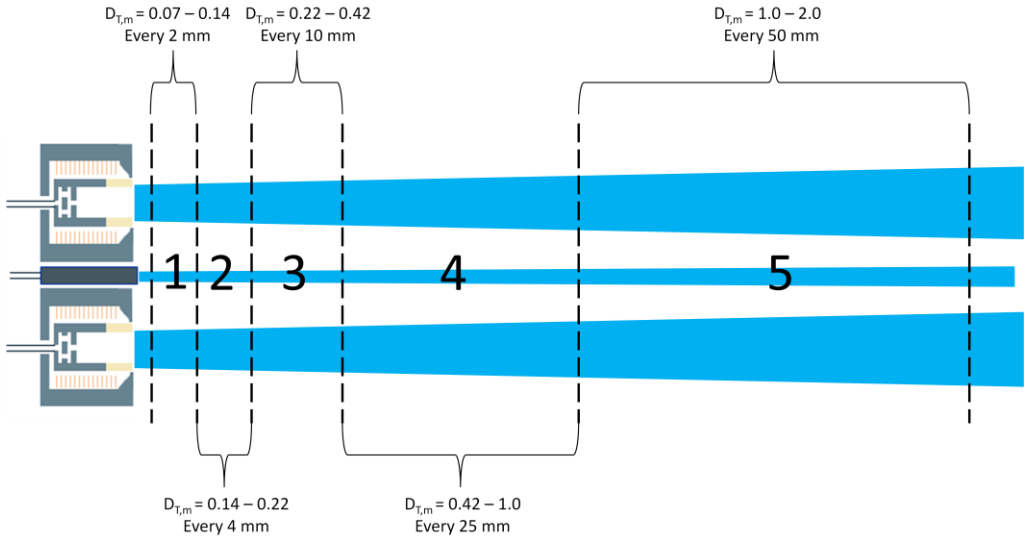

Figure 2. Diagram detailing axial spatial resolution as a function of downstream distance from the thruster exit plane. Resolution becomes more coarse as the probes move further downstream where gradients are expected to be small. Not to scale.

The following sections detail the probe construction, measurement circuits, and data analysis techniques associated with the single Langmuir probe and emissive probe.

1. Langmuir Probe

A single Langmuir probe was used in this study to measure floating potential and electron temperature in the near-field plume of the NASA-300M. Figure 3 shows a schematic of the tip of the probe used in this study. The probe itself was comprised of a 0.250-mm-diameter pure tungsten wire sleeved within a double-bore alumina tube with an outer diameter of 3.2 mm. The exposed length of the wire was 2.0 mm, providing a length-to-diameter ratio of eight to reduce end effects. An identical wire was sleeved in the adjacent bore and encapsulated by high-temperature ceramabond to isolate it from the plasma. This "null" probe was biased in the same way as the "active" probe, but due to its isolation from the plasma can characterize the capacitive currents in the electrical line that can be subtracted out in data post-processing.[11] The majority of the lines leading from the probe wires to the measurement circuit were comprised of shielded coaxial cabling.

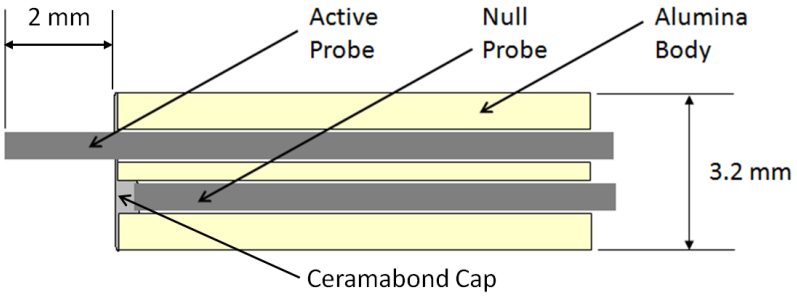

Figure 3. Schematic of the tip of the Langmuir probe used in this study. An encapsulated null probe was included to characterize line capacitive effects. Not to scale.

Figure 4 shows a schematic of the measurement circuit used for the single Langmuir probe. Two 160-Ω, 1-W carbon resistors were used as shunts to measure the current from the active and null probes. The voltages from the shunts were passed through voltage-following isolation amplifiers to protect the data acquisition system (DACS) from high common-mode voltages. Blocking diodes were also placed across the shunts to protect the circuitry from any large current spikes. Voltage was applied to the probes via a bipolar power supply connected to a function generator. The applied voltage was measured using a voltage divider comprised of 10-MΩ and 0.83-MΩ 0.25-W metal-film resistors, whose voltage signal was also passed through a voltage-following isolation amplifier. For this study, the applied voltage was a symmetric triangle wave with a frequency of 125 Hz, well within the 20-kHz bandwidth of the isolation amplifiers. This sweep rate provided a radial spatial resolution of 1.0-1.5 mm, depending on the radial motion table speed. The probe voltage range was fixed at approximately -85 to +15 V with respect to facility ground throughout the entire study. Both current and voltage signals were measured using a 16-bit commercially available DACS. The circuit was calibrated both before and after the study, and displayed excellent linearity and repeatability. The scan rate across each channel was 75 kHz for most of the operating conditions tested, resulting in 300 data points per Langmuir probe I-V characteristic. However, the scan rate at 300 V and 10 kW was reduced to 50 kHz, resulting in 200 data points per I-V characteristic. The scan rate was determined primarily by the radial table speed since the total number of points taken was kept fixed at the maximum possible value the DACS buffer could hold (i.e. 500,000 points).

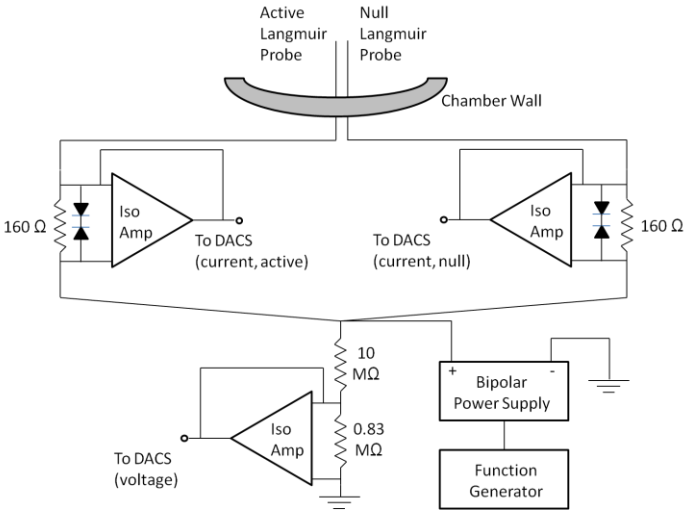

Figure 4. Electrical diagram of the measurement circuit used for the Langmuir probe in this study.

Data analysis of each I-V characteristic largely followed simple Langmuir probe theory.[12,13] First the floating potential was found by locating the probe voltage at which zero net current was collected. The ion current was then subtracted from the trace and a natural logarithm of the resulting electron current was plotted against probe voltage. A fit was made using linear regression to the region around the floating potential, whose inverse slope was taken to be the electron temperature in eV. Due to variations in line fits to the data, uncertainty in the electron temperature is estimated at ±15%.

It should be noted that for several operating conditions the null probe current exhibited erratic behavior that prevented it from directly being used to compensate for line capacitance. In these instances, the portions of the current that behaved as expected were used to directly calculate the line capacitance itself using

$$I_{cap} = C\frac{dV}{dt}, \tag{2}$$

where I_{cap} is the capacitive current, C is the line capacitance, and dV/dt is the time rate of change of the applied probe bias. Figure 5 shows an example of measured null probe current when well-behaved. Typical values of calculated capacitance were approximately 2 nF. These values were then used along with the calculated dV/dt to calculate and subtract out capacitive line currents, which worked well in the instances when the null probe current could not be directly used (i.e. no shifts in collected current on the active probe were observed at locations where *dV/dt* changed sign).

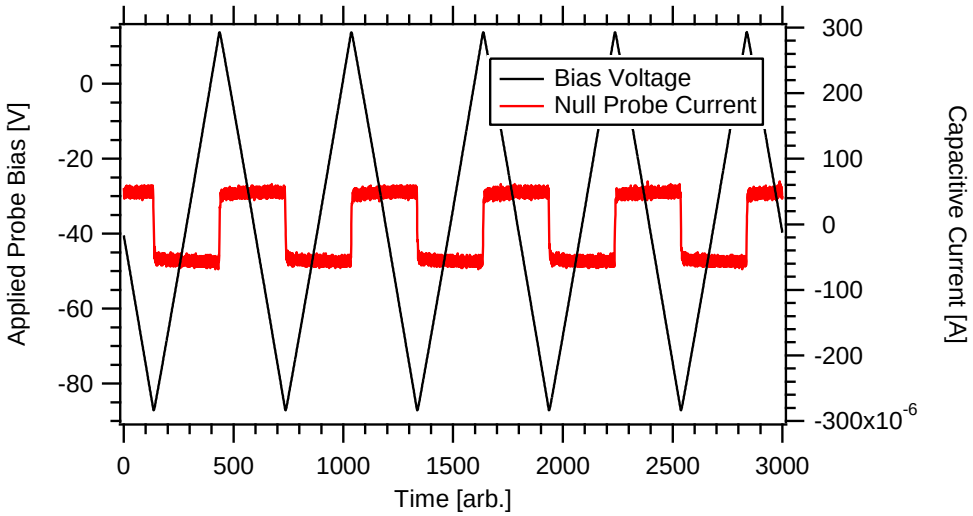

Figure 5. Example of null probe response to probe bias when well-behaved. The triangle waveform for voltage resulted in a square wave of null probe current, as expected based on Eq. (2).

2. Emissive Probe

A floating emissive probe was used in this study to measure the local plasma potential in the near-field plume of the NASA-300M. This type of probe has extensive heritage measuring plasma potentials inside the channel as well as in the near-field plume of Hall thrusters.[14-17] It is an attractive diagnostic due to its simple operation, direct measurement technique, and insensitivity to various non-ideal environmental factors such as the presence of magnetic fields and non-Maxwellian electron populations. The probe design for this study was based on the design by Haas[14] and later augmented by Linnell[16] and Reid.[17] The probe filament was comprised of a 0.102-mm-diameter 1% thoriated tungsten wire with a radius of curvature of 0.8 mm. The filament was inserted into a double-bore alumina tube with an outer diameter of 3.2 mm. Pure tungsten wire 0.250 mm in diameter was used as lead wires and interfaced with the filament inside the alumina tube via an interference "press" fit. Additional tungsten "filler" wires were inserted into the tube to ensure a tight fit and proper electrical contact between the filament and lead wires. The final length of the emissive probe filament (distance from tube end to filament tip) was 1.6 mm (see Fig. 6).

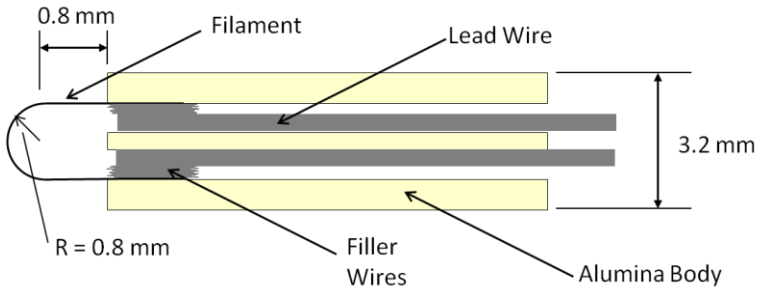

Figure 6. Schematic of the emissive probe tip used in this study. Not to scale.

Figure 7 shows the measurement circuit used to measure the potential of the emissive probe. A floating power supply was used to supply the necessary current, typically between 2 and 2.5 A, to heat the filament to proper levels of thermionic emission. The potential on either side of the probe was measured to reduce uncertainties associated with the potential drop across the filament, which varied from 3 - 7 V. Each potential was measured using a voltage divider comprised of 10-MΩ and 0.81-MΩ 0.25-W metal film resistors. The signal of each measurement was sent through a voltage-following isolation amplifier before being read by the same DACS that monitored signals from the Langmuir probe circuit. The voltage dividers were calibrated both before and after the study, and displayed excellent linearity and repeatability.

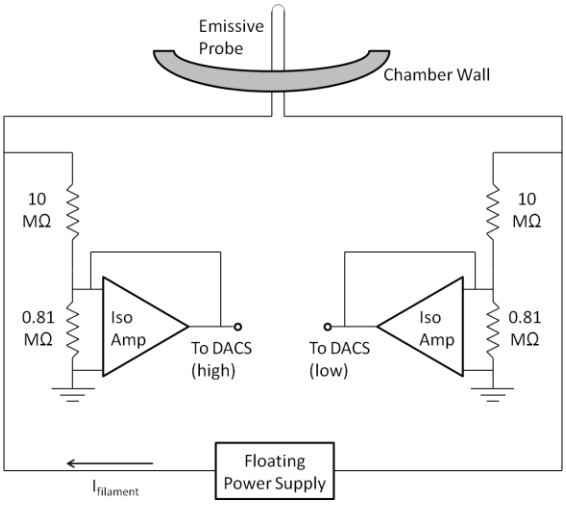

Figure 7. Electrical schematic of the measurement circuit used with the emissive probe in this study.

The proper level of filament current was determined by monitoring the potential of the filament across the thruster face at the closest axial position in the interrogation map, while slowly increasing the supplied current with each pass. The proper level was chosen as the minimum required current at which the signal no longer changed with any increase in current. This current was then used for the entire spatial map at the given operating condition. When not in use in between radial sweeps, the filament current was set to a low value (where the probe was emitting but not strongly) to minimize thermal loading and premature failure of the probe while avoiding large thermal cycling*.

Data analysis comprised of averaging the high and low measured potentials from the DACS. Based on the work of Linnell,[16] a correction factor of $0.6T_e$ was added to the average measured potential to correct for space-charge-limited effects at the probe surface. Each radial sweep was downsampled to 2000 points, resulting in a radial spatial resolution of approximately 1 mm. This was done to control the large data sets resulting from the 50-75 kHz sampling rate dictated by the Langmuir probe data collection.

III. Results

An electrostatic probe array was used to measure floating potential, electron temperature, and local plasma potential in the near-field plume of the NASA-300M Hall thruster. Four of the operating conditions tested are presented in this work: 300 V at 10 and 20 kW, 400 V at 20 kW, and 500 V at 20 kW. While the interrogation zone included data up to 4 $D_{T,m}$ radially away from thruster centerline, only data within ±1 $D_{T,m}$ is presented here. This was done because properties exhibited almost zero gradient far off-axis. Furthermore, the analysis of the data in this region was more sensitive to noise due to smaller signals resulting from low plasma density. Spatial mapping of the plasma potential and electron temperature are presented in the following sections.

A. Plasma Potential

Since one of the primary goals of this study is to obtain data for validation of ongoing modeling efforts at GRC and JPL,[9] the nominal operating condition of 500 V at 20 kW was considered critical to characterize in terms of

*Personal Communication (email) with D.M. Goebel.

capturing the location of the acceleration zone. For this reason, both emissive probes were operated to failure at this operating condition in an effort to obtain data as close as possible to the thruster exit plane. Thus, no other plasma potential data is available at the other operating conditions. Figure 8 shows the contour map of plasma potential at this operating condition. All values reported are with respect to cathode potential – measurements with respect to ground have been corrected with the measured cathode-to-ground potential, typically between -5 and -10 V. Values below zero, typically measured near the center-mounted cathode, have been removed from the contour. Due to the extremely high current densities in this region, it is likely that the emissive probe was not emitting strongly enough to properly float up to the local plasma potential. Attempts to properly measure plasma potential by the cathode would have most likely resulted in probe failure.

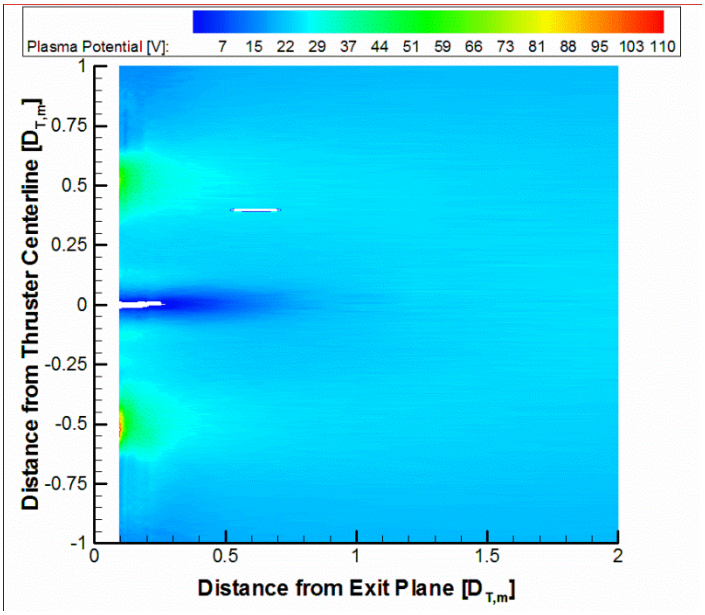

Figure 8. Contour map of plasma potential in the near-field plume at 500 V and 20 kW. Most of the acceleration zone captured is within 0.2 $D_{T,m}$ of the thruster exit plane. All values reported are with respect to cathode potential.

It is evident from the figure that the plasma potential is fairly uniform throughout most of the near-field plume. Most of the acceleration zone that was captured lies within 0.2 $D_{T,m}$ of the thruster exit, while the remainder of the plume is at 20-30 V above cathode potential. The maximum measured plasma potential at 0.1 $D_{T,m}$ from the exit plane is approximately 96 V. This confirms that while near-field plume studies provide critical information about the plasma just downstream of the exit plane, internal measurements are necessary to capture the majority of the acceleration zone. Symmetry between the two sides of the channel as well as the acceleration zone location itself is further discussed in Section IV.

B. Electron Temperature

Figure 9 shows contour maps of the measured electron temperature in the near-field plume of the NASA-300M at four operating conditions. All four maps have been plotted on the same scale for comparison. It is evident from the figure that the isothermal lines exhibit similar structure across all four operating conditions presented. The source of this structure and its implications are further discussed in Section IV. At all four operating conditions, the high-temperature region is contained within 0.3 $D_{T,m}$ of the thruster exit plane. Afterwards, the electron temperature is fairly uniform in the near-field plume at approximately 2 – 5 eV depending on the operating condition. The maximum measured electron temperatures at 0.07 $D_{T,m}$ from the exit plane are: 27 eV at 500 V and 20 kW, 22 eV at 400 V and 20 kW, 23 eV at 300 V and 20 kW, and 19 eV at 300 V and 10 kW. While higher electron temperatures are expected at higher discharge voltages due to increased Ohmic heating, changes in the location of the ionization and acceleration zones introduce additional factors that affect the maximum electron temperature seen in the near-field plume. As will be seen in Section IV, these temperatures have a strong influence over behavior near surfaces adjacent to the channel exit (i.e. the channel walls and magnetic poles).

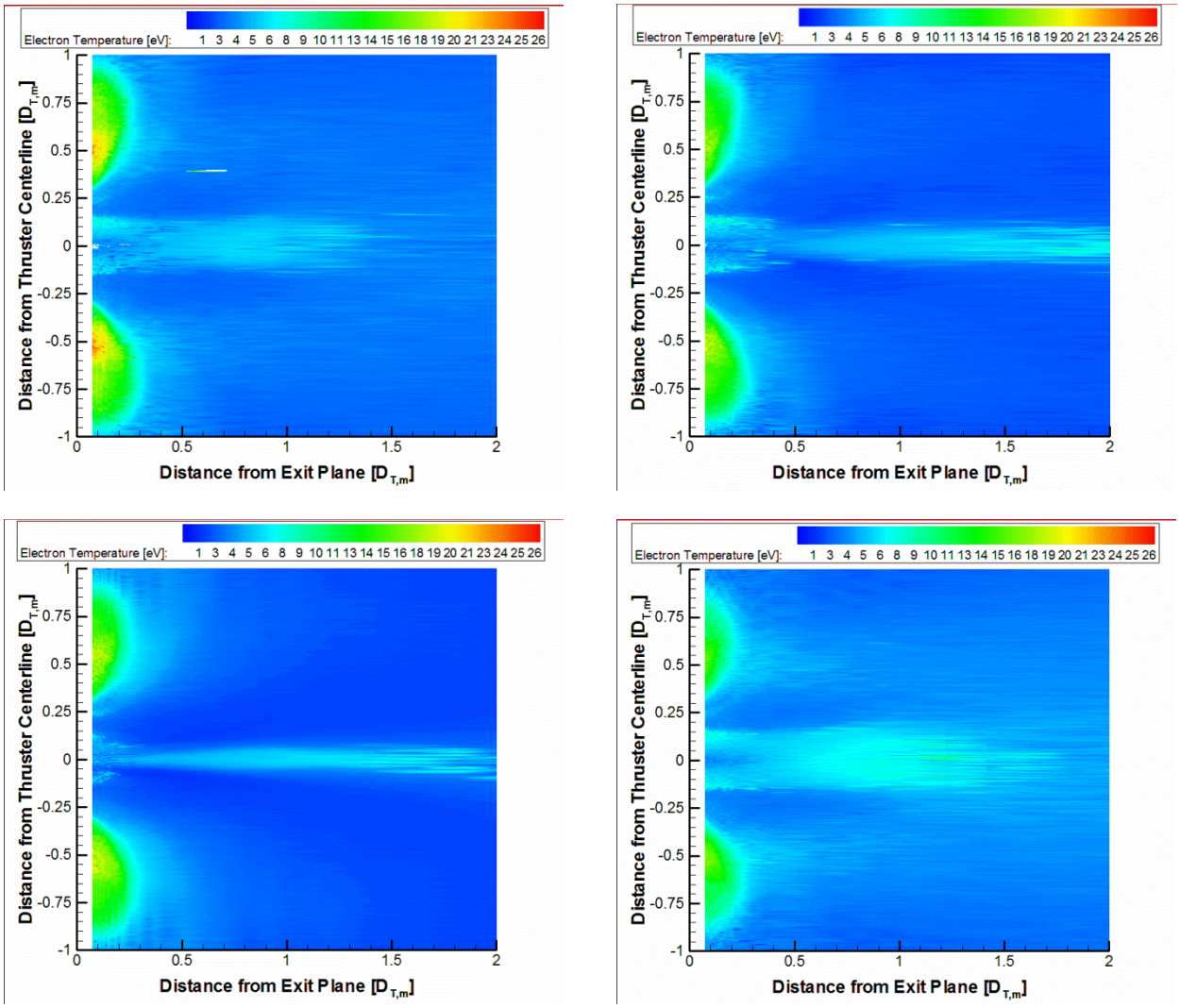

Figure 9. Contour maps of electron temperature in the near-field plume of the NASA-300M. Top Left: 500 V at 20 kW. Top Right: 400 V at 20 kW. Bottom Left: 300 V at 20 kW. Bottom Right: 300 V at 10 kW. All four operating conditions exhibit similar structure in their isothermal lines.

IV. Discussion

An electrostatic probe array was used to measure the floating potential, plasma potential, and electron temperature in the near-field plume of the NASA-300M. Section III results have shown that the majority of the acceleration zone and high-temperature regions are limited to 0.3 $D_{T,m}$ downstream of the thruster exit plane. Based on these results, four topics will be discussed in this section. The first is the source and implications of the structure of isothermal lines in the near-field plume. The second is behavior near the exit plane channel walls and magnetic poles as a result of the electron temperature spatial distribution. The third is a closer analysis of the acceleration and high-temperature regions (the very-near-field plume) at all four operating conditions. Lastly, due to the nature of the interrogation map, symmetry between the two measured sides of the thruster will be briefly discussed.

A. Isothermal Line Structure

As seen in Section III, the shape of isothermal lines in the near-field plume all exhibited a similar shape and structure between the four operating conditions presented despite the change in discharge voltage, anode mass flow rate, and discharge power. To examine this structure further, the electron temperature is plotted at 0.07 $D_{T,m}$ from the exit plane at each operating condition (see Fig. 10). The electron temperature tended to peak at channel centerline (± 0.5 $D_{T,m}$), while rapidly falling off as the center-mounted cathode is approached (0 $D_{T,m}$). The falloff is

much more gradual when moving radially outwards beyond channel centerline. While the magnitude of electron temperature changes across operating conditions, the shape itself appears to be consistent. This is even more apparent when the profiles are non-dimensionalized by the maximum measured electron temperature at each operating condition (see Fig. 11).

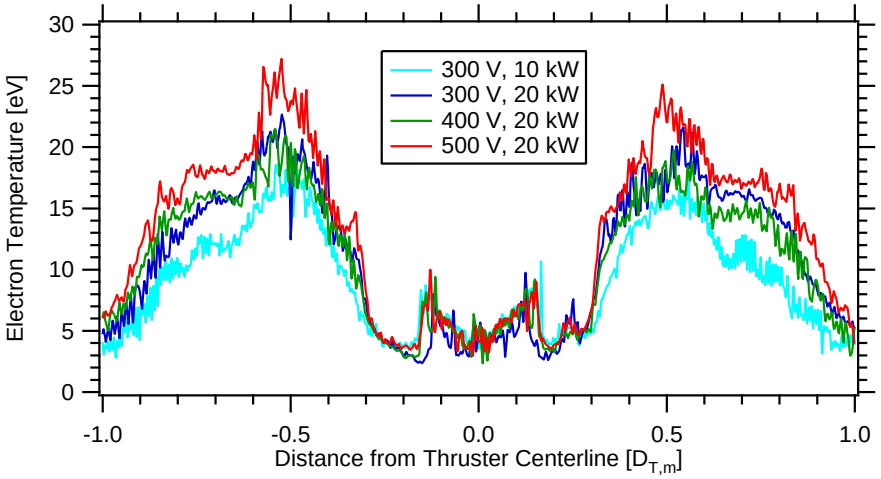

Figure 10. Electron temperature as a function of radial position at 0.07 $D_{T,m}$ from the thruster exit plane. Each profile has a distinct shape that appears to be consistent across operating conditions.

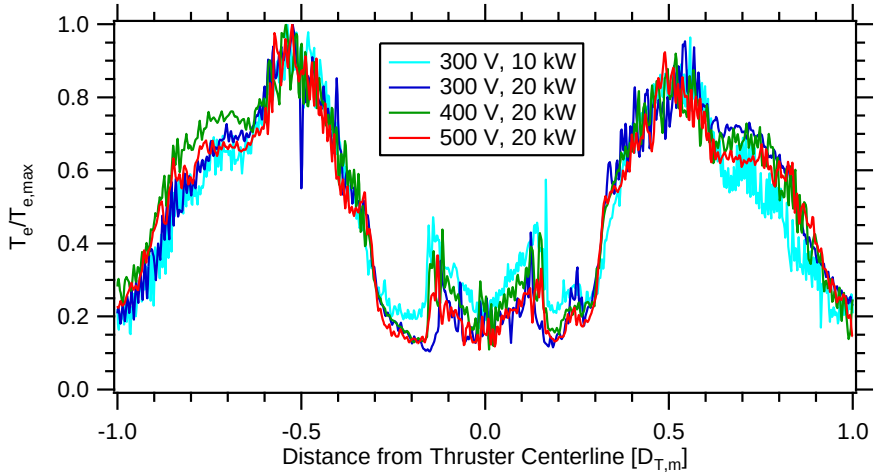

Figure 11. Radial profiles of electron temperature at 0.07 $D_{T,m}$ from the thruster exit plane, non-dimensionalized by the maximum electron temperature at each operating condition. It is evident that the profiles share an identical structure despite variations in throttling parameters.

The lobe-like structure seen in the contour maps in Fig. 9 are strongly reminiscent of the magnetic field topology in the near-field region of Hall thrusters. Figure 12 illustrates the similarity between the magnetic field topology of the NASA-173Mv1,[18] which exhibits a similar shape to the NASA-300M topology but is not restricted for public release, and the measured electron temperature contours at 500 V and 20 kW. Given the seemingly universal structure of the electron temperature and the fact that the magnetic field topology was not changed throughout the study, it is reasonable to conclude the magnetic field lines are shaping the isothermal lines in the near-field plume. This is further experimental evidence for computational studies that typically assume that magnetic field lines have constant electron temperature. Furthermore, this trend will be important to verify once a magnetically-shielded version of the 300M is fabricated and these measurements are taken again on the new test article. The isothermal lines are expected to be well-defined due to the distinctive topology associated with magnetically-shielded Hall thrusters.[8]

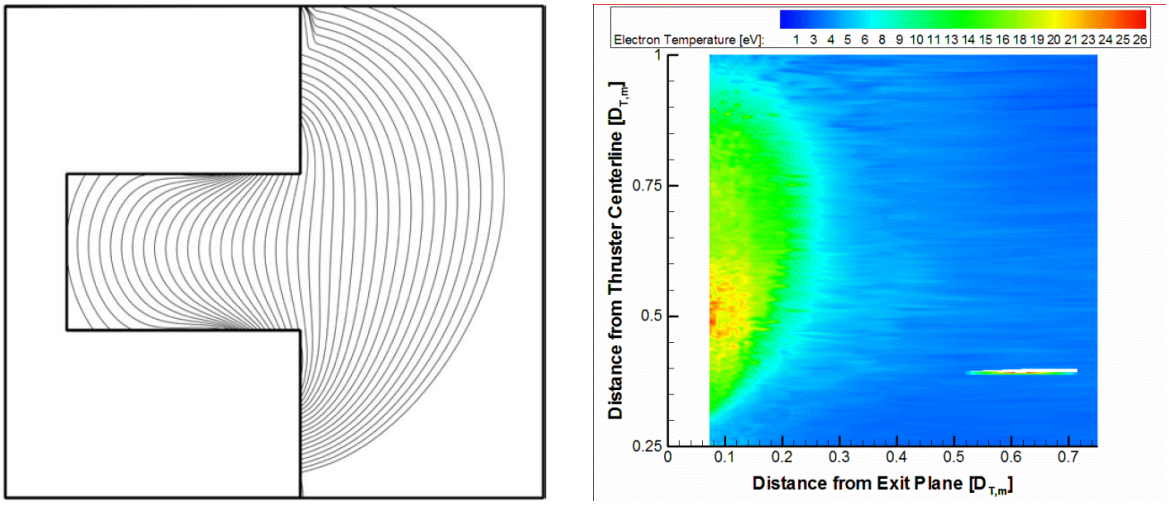

Figure 12. Comparison of magnetic field topology from the NASA-173Mv1[18] (left) with measured electron temperature of the NASA-300M at 500 V and 20 kW (right). The field shape from the NASA-173Mv1 represents a similar field shape to the one used on the 300M, and exhibits similar structure to the observed electron temperature contours.

B. Behavior at Surfaces Adjacent to Channel

The distinctive shape of isothermal lines has implications for the behavior of potentials in the vicinity of surfaces adjacent to the channel exit plane. Since the isothermal lines appear to follow magnetic field lines, the magnetic field topology tends to draw the high-temperature region downstream of the channel towards the magnetic pole surfaces as well as the insulator surfaces comprising the channel exit plane. However, these regions are also characterized by a low, relatively constant plasma potential due to a lack of dense plasma in these regions.[4] The combination of these two factors results in a significant drop in the local floating potential in these areas. Figure 13 shows a contour map of the measured floating potential at the nominal condition of 500 V and 20 kW. All floating potentials reported are with respect to facility ground. It is evident from the figure that the regions adjacent to the channel bounds have very low floating potentials, on the order of -80 V.

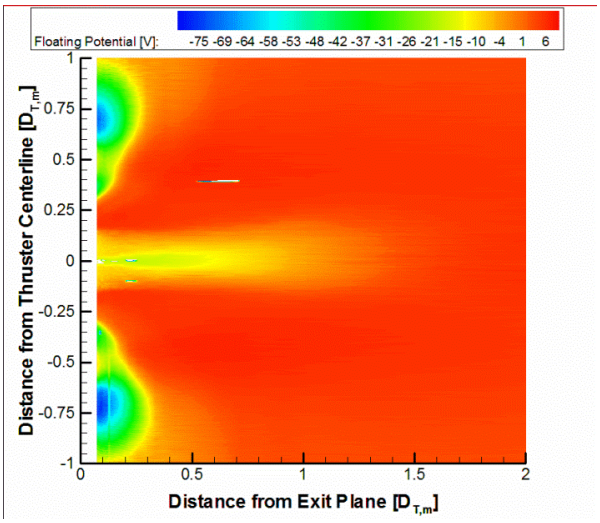

Figure 13. Contour map of the measured floating potential in the near-field plume at 500 V and 20 kW. All potentials are with respect to facility ground. Areas adjacent to the channel bounds are characterized by floating potentials on the order of -80 V.

The degree to which this potential drop occurs is a strong function of the electron temperature values in this region. Figure 14 shows radial profiles of the measured floating potential at 0.07 $D_{T,m}$ from the thruster exit plane.

It is evident that the floating potential drops are more significant for operating conditions that have higher electron temperatures near the exit plane. These radial profiles also show that while floating potential drops exist on both sides of the channel, the one on the outside is much more significant. The reason for this is evident from Fig. 10. Due to the magnetic field topology (field lines are more concentrated towards the inner pole), the electron temperature falls off much more rapidly from channel centerline when moving radially inward than when moving outward. This causes the region of high electron temperatures to be wider in the radial direction on the outer side of the channel, thus allowing the number density and plasma potential to decrease substantially in these regions and create a larger low-density, high-temperature area.

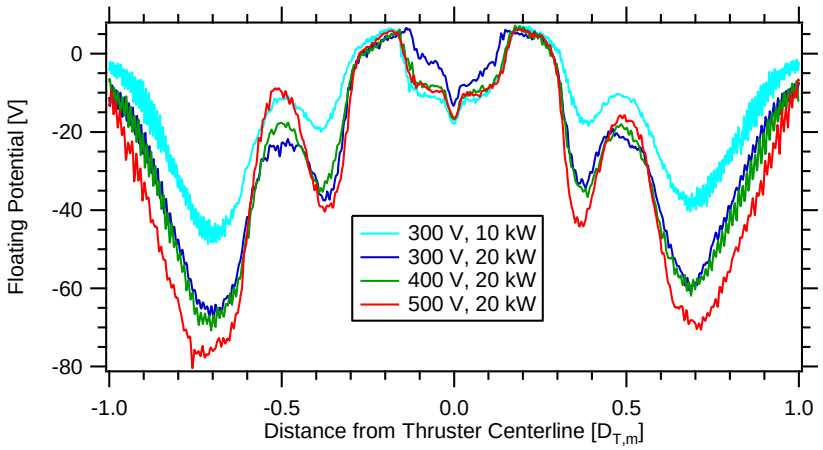

Figure 14. Radial profiles of measured floating potential 0.07 $D_{T,m}$ from the thruster exit plane. More significant drops in floating potential are found for operating conditions that have higher electron temperatures in this region.

The implications, if any, on thruster performance are unclear at this time. Having a low-density, high-temperature plasma in the vicinity of the magnetic poles indicates that the sheaths formed on these surfaces will be thick with large potential drops. However, the power losses are not expected to be significant due to the lack of significant plasma in these regions. It is worth noting from an experimental point of view that this trend was unexpected when the tests were performed. Thus, in these regions the Langmuir probe and Faraday probe were not biased sufficiently low enough to properly measure ion saturation current. In future studies this phenomenon will have to be accounted for to obtain a more complete data set in these regions.

C. Analysis of the Very-Near-Field Plume

It was shown in Section III that the majority of the acceleration zone and high-temperature regions were contained within 0.3 $D_{T,m}$ of the thruster exit plane. For this work, this region will be referred to as the very-near-field plume. The rise in electron temperature and plasma potential with axial distance as the exit plane is approached will be discussed in more detail in this section.

Figures 15 and 16 show the axial profiles at channel centerline (-0.5 $D_{T,m}$) of the measured plasma potential at 500 V and 20 kW as well as the electron temperatures at the four operating conditions presented. Distance is plotted on a log scale to better illustrate the sharp rise in properties within 0.3 $D_{T,m}$ of the thruster exit plane. The locations where the plasma potential and electron temperature begin to rise as the exit plane is approached correspond to each other. Assuming the plasma potential reaches anode potential deep in the channel, only 15% of the potential rise towards anode has occurred 0.1 $D_{T,m}$ from the exit plane. This is somewhat surprising given that the electron temperature has risen to 21 eV at this axial location, indicating an average gain of 0.25 eV/V of potential. It has been well-established that electron temperature tends to vary linearly with plasma potential.[16,17,19] These prior measurements have shown over multiples thrusters and diagnostics that typical values of electron temperature gain are 0.07 – 0.16 eV/V of potential over a significant fraction of the acceleration zone, much lower than what is observed in this study. It is possible that net electron heating is higher in the near-field plume, and that heating within the channel would be partially suppressed with increased losses associated with the channel walls.[19] However, measurements internal to the channel currently being made at GRC will help better understand how the potential and temperature rise towards the anode in the 300M.

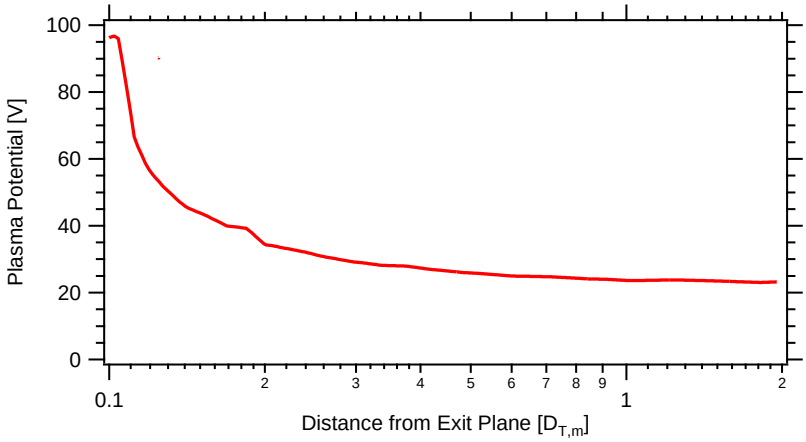

Figure 15. Measured plasma potential at channel centerline (-0.5 $D_{T,m}$) as a function of axial distance for 500 V and 20 kW. Distance is given on a log scale to better display the sharp rise in plasma potential near the thruster exit plane. Maximum measured potential is 96 V with respect to cathode potential.

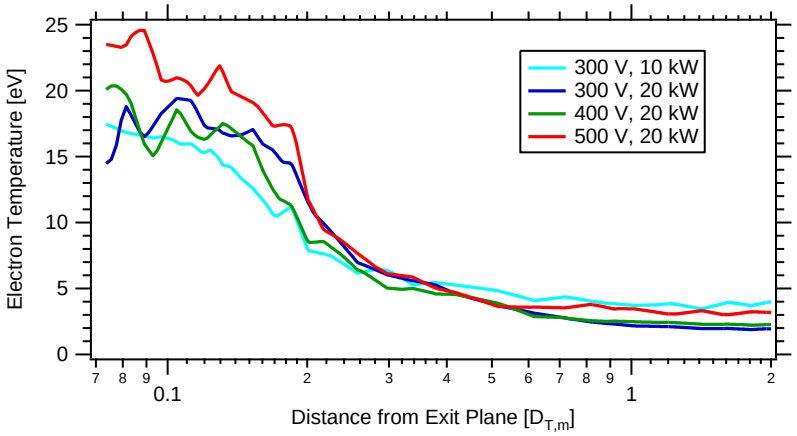

Figure 16. Axial profiles of the electron temperature at channel centerline (-0.5 $D_{T,m}$). Distance is given on a log scale to better illustrate the sharp rise in temperature as the exit plane is approached.

If the maximum electron temperature is assumed to be 0.1 the discharge voltage,[14] at 0.07 $D_{T,m}$ from the exit plane, the electron temperature has reached: 47% of its maximum at 500 V, 20 kW; 50% of its maximum at 400 V, 20 kW; 48% of its maximum at 300 V, 20 kW; and 58% of its maximum at 300 V, 10 kW. Given the fact that the temperature rise occurs at approximately the same location (between 0.2 and 0.3 $D_{T,m}$), there is a large amount of similarity between the electron temperature profiles. This is more apparent when the profiles are non-dimensionalized by the maximum electron temperature (see Fig. 17). This result is surprising as these profiles are influenced by the acceleration zone length and location, which are expected to change with operating condition.[17,19] Once again, more data is required to better understand the trends between plasma potential and electron temperature profiles in the 300M.

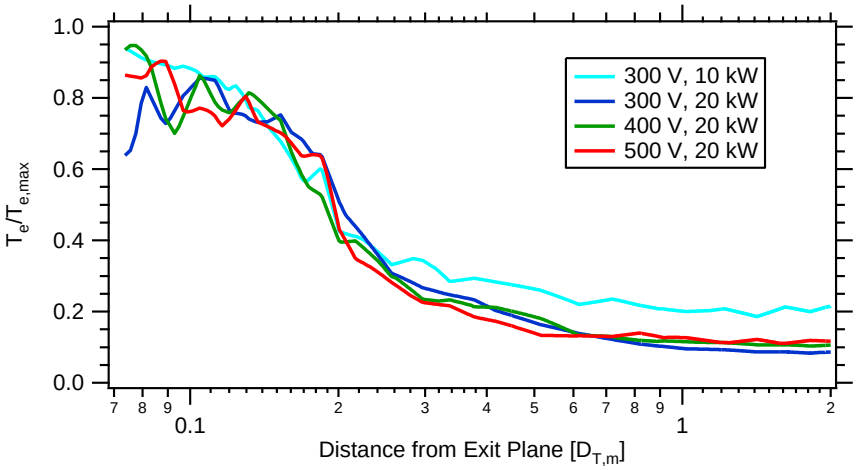

Figure 17. Axial profiles of electron temperature non-dimensionalized by the maximum electron temperature at each operating condition. Similar structure is once again found across operating conditions.

D. Symmetry between Thruster Sides

Since both sides of the thruster were interrogated in this study, it is worth comparing the two channels to verify the frequent assumption of azimuthal symmetry. Figure 18 shows the radial profile of measured plasma potential at 0.1 $D_{T,m}$ from the exit plane at 500 V and 20 kW. It is evident that there is not perfect symmetry between the two channels. The peak potential at -0.5 $D_{T,m}$ (9 o'clock position when facing the thruster) is 96 V while the peak potential at +0.5 $D_{T,m}$ (3 o'clock position when facing the thruster) is 66 V. However, this does not necessarily indicate a large degree of asymmetry. Figure 19 compares the axial profiles of plasma potential between clocked positions at 500 V and 20 kW. Due to the sharp gradient in potential near the exit plane, a slight axial shift in acceleration zone could create significant potential differences between clocked positions at a given axial location. In fact, a shift of just 0.013 $D_{T,m}$ in the profile at the 3 o'clock position would create excellent agreement and symmetry between the two sides. It is worth noting that a slight misalignment between the radial motion table and the thruster exit plane could also explain the asymmetry, since the necessary axial shift corresponds to only 0.75°. Therefore, it is reasonable to conclude that the two sides of the thruster are symmetric within the alignment uncertainty of the probe motion system.

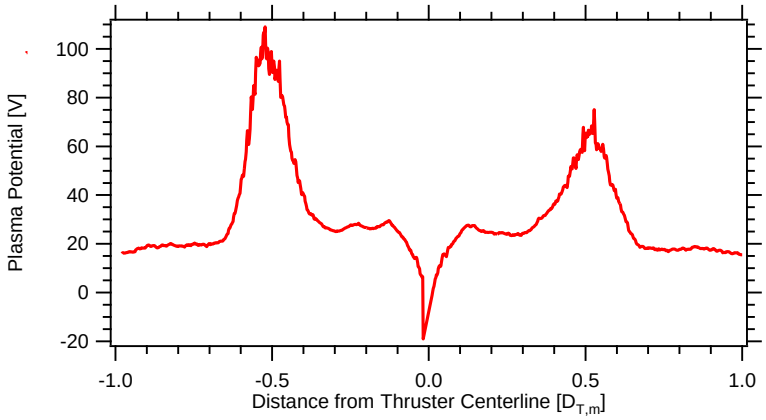

Figure 18. Radial profile of plasma potential at 0.1 $D_{T,m}$ from the exit plane at 500 V and 20 kW. The two sides of the thruster do not appear to be perfectly symmetric, with peak potentials being different by 30 V. However, these differences were determined to be within thruster and motion table alignment uncertainties.

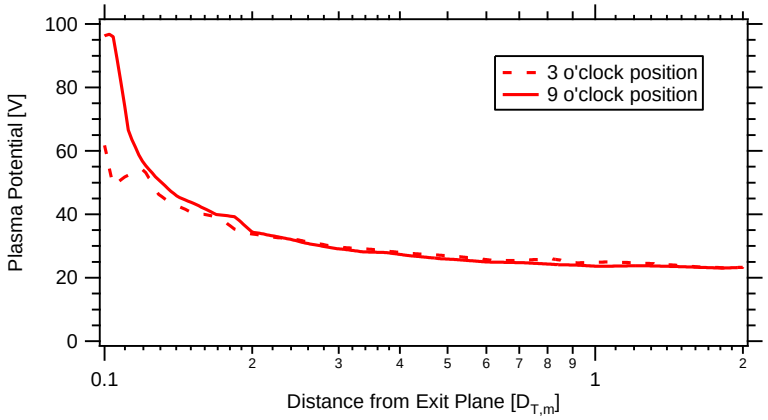

Figure 19. Axial profiles of plasma potential at channel centerline between the 3 o'clock and 9 o'clock position at 500 V and 20 kW. Due to the steep rise in plasma potential as the exit plane is approached, a significant difference in potential could exist between clocked positions based on a small axial shift in acceleration zone (0.013 $D_{T,m}$).

V. Conclusions

An electrostatic probe array was used to measure the local floating potential, plasma potential, and electron temperature in the near-field plume of the NASA-300M Hall thruster. Measurements have shown that the acceleration zone and high-temperature regions are limited to approximately 0.3 $D_{T,m}$ from the thruster exit plane for all four operating conditions presented. Electron temperature spatial distributions were found to be similar across operating conditions and were strongly shaped by the magnetic field topology. Maximum measured electron temperatures in the near-field varied between 19 and 27 eV depending on operating condition. The magnetic field shape carried the high-temperature region downstream of the channel towards the front surfaces of the magnetic poles, creating a region of very low floating potential that suggests strong sheath formation on these surfaces. Comparison between the two interrogated sides of the thruster suggested azimuthal symmetry within the alignment uncertainty associated with the probe motion system. The data taken in this study have provided valuable information for validation of ongoing modeling efforts, future design of high-power Hall thrusters, and comparison with ongoing internal measurements on the NASA-300M at NASA GRC.

Acknowledgments

The authors would like to thank and acknowledge the Office of the Chief Technologist for funding this work as well as Timothy Smith for serving as Project Manager. The authors would also like to thank Thomas Haag and Kevin McCormick for their aid in designing and building the probe mount used in this study, George Readus for installing the probe motion system used, as well as George Jacynycz and Kevin Blake for maintaining and operating the vacuum facility.

References

[1]Peterson, P. Y., Jacobson, D. T., Manzella, D. H., and John, J. W., "The Performance and Wear Characterization of a High-Power High-Isp NASA Hall Thruster," Presented at the 41st AIAA/ASME/SAE/ASEE Joint Propulsion Conference and Exhibit, AIAA-2005-4243, Tucson, AZ, July 10 - 13, 2005.

[2]Manzella, D., Jankovsky, R., and Hofer, R. R., "Laboratory Model 50 kW Hall Thruster," Presented at the 38th AIAA/ASME/SAE/ASEE Joint Propulsion Conference and Exhibit, AIAA-2002-3676, Indianapolis, IN, July 7-10, 2002.

[3]Jacobson, D. T., Manzella, D. H., Hofer, R. R., and Peterson, P. Y., "NASA's 2004 Hall Thruster Program," Presented at the 40th AIAA/ASME/SAE/ASEE Joint Propulsion Conference and Exhibit, AIAA-2004-3600, Fort Lauderdale, Florida, July 11-14, 2004.

[4]Huang, W., Shastry, R., Herman, D. A., Soulas, G. C., and Kamhawi, H., "Ion Current Density Study of the NASA-300M and NASA-457M v2 Hall Thrusters," Presented at the 48th AIAA/ASME/SAE/ASEE Joint Propulsion Conference and Exhibit, Atlanta, GA, July 29 - August 1, 2012.

[5]Kamhawi, H., Haag, T. W., Jacobson, D. T., and Manzella, D. H., "Performance Evaluation of the NASA-300M 20 kW Hall Effect Thruster," Presented at the 47th AIAA/ASME/SAE/ASEE Joint Propulsion Conference and Exhibit, AIAA-2011-5521, San Diego, CA, July 31 - August 3, 2011.

[6]Shastry, R., Huang, W., Herman, D. A., Soulas, G. C., and Kamhawi, H., "Plasma Potential and Langmuir Probe Measurements in the Near-field Plume of the NASA 457Mv2 Hall Thruster," Presented at the 48th AIAA/ASME/SAE/ASEE Joint Propulsion Conference and Exhibit, Atlanta, GA, July 29 - August 1, 2012.

[7]Soulas, G. C., Haag, T. W., Herman, D. A., Huang, W., Kamhawi, H. et al., "Performance Test Results of the NASA-457M v2 Hall Thruster," Presented at the 48th AIAA/ASME/SAE/ASEE Joint Propulsion Conference and Exhibit, Atlanta, GA, July 29 - August 1, 2012.

[8]Mikellides, I. G., Katz, I., Hofer, R. R., Goebel, D. M., De Grys, K. et al., "Magnetic Shielding of the Acceleration Channel Walls in a Long-Life Hall Thruster," Presented at the 46th AIAA/ASME/SAE/ASEE Joint Propulsion Conference and Exhibit, AIAA-2010-6942, Nashville, TN, July 25 - 28, 2010.

[9]Mikellides, I. G., Katz, I., Kamhawi, H., and Vannoord, J. L., "Numerical Simulations of a 20-kW Class Hall Thruster Using the Magnetic-Field-Aligned-Mesh Code Hall2De," Presented at the 32nd International Electric Propulsion Conference, IEPC-2011-244, Wiesbaden, Germany, September 11-15, 2011.

[10]Jameson, K. K., Goebel, D. M., Hofer, R. R., and Watkins, R. M., "Cathode Couplings in Hall Thrusters," Presented at the 30th International Electric Propulsion Conference, IEPC-2007-278, Florence, Italy, September 17-20, 2007.

[11]Lobbia, R. B. and Gallimore, A. D., "High-speed dual Langmuir probe," *Review of Scientific Instruments* 81, 7, 073503-1 - 073503-9 (2010).

[12]Hershkowitz, N., in *Plasma Diagnostics: Discharge Parameters and Chemistry*, edited by Flamm, D. L. (Academic Press, Inc., 1989), pp. 113-181.

[13]Lieberman, M. A. and Lichtenberg, A. J., *Principles of Plasma Discharges and Materials Processing*, Second ed. (John Wiley & Sons, Inc., Hoboken, NJ, 2005).

[14]Haas, J. M., "Low-Perturbation Interrogation of the Internal and Near-Field Plasma Structure of a Hall Thruster Using a High-Speed Probe Positioning System," Ph.D. Dissertation, Aerospace Engineering, University of Michigan, 2001.

[15]Jameson, K. K., "Investigation of Hollow Cathode Effects on Total Thruster Efficiency in a 6 kW Hall Thruster," Ph.D. Dissertation, Aerospace Engineering, University of California Los Angeles, 2008.

[16]Linnell, J. A., "An Evaluation of Krypton Propellant in Hall Thrusters," Ph.D. Dissertation, Aerospace Engineering, University of Michigan, 2007.

[17]Reid, B. M., "The Influence of Neutral Flow Rate in the Operation of Hall Thrusters," Ph.D. Dissertation, Aerospace Engineering, University of Michigan, 2008.

[18]Hofer, R. R., "Development and Characterization of High-Efficiency, High-Specific Impulse Xenon Hall Thrusters," Ph.D. Dissertation, Aerospace Engineering, The University of Michigan, 2004.

[19]Raitses, Y., Staack, D., Smirnov, A., and Fisch, N. J., "Space charge saturated sheath regime and electron temperature saturation in Hall thrusters," *Physics of Plasmas* 12, 7, 073507-1 - 073507-10 (2005).